ORIGINAL PAPER

A source and ground motion study of earthquakes in and near Delhi (the National Capital Region), India

Brijesh K. Bansal[1,2] ⬤ · **S. K. Singh[3]** · **G. Suresh[1]** · **H. Mittal[1]**

© The Author(s), under exclusive licence to Springer Nature B.V. 2021

Abstract

We study source parameters of 10 local earthquakes ($2.7 \leq M_w \leq 4.5$) that have occurred in the National Capital Region (NCR) since 2001 and the ground motions produced by these events. Moment rate spectra of the earthquakes retrieved from the recordings at hard sites after applying corrections for geometrical spreading ($1/R$, $R \leq 100$ km), anelastic attenuation ($Q = 253f^{0.8}$) and cutoff frequency ($f_m = 35$ Hz) are reasonably well fit by the Brune ω^2-source model with stress drop ranging between 0.9 and 13 MPa. Neglecting the outlier low-stress drop value, the average stress drop is 6 MPa. We apply a modified standard spectral ratio technique to estimate site effect at 38 soft sites in the NCR as well as the geometrical mean site effect with respect to a reference hard site. Application of the stochastic method, with source characterized by the Brune ω^2- model with stress drop of 6 MPa and the mean site effect for soft sites, yields peak horizontal ground acceleration and velocity curves that are in good agreement with the observed values. These results provide the parameters needed for the application of the stochastic method to predict ground motions at hard and soft sites in the NCR during postulated $M_w \leq 5.5$ earthquakes.

Keywords Delhi earthquakes · Ground motion prediction · National Capital Region · Site effect

1 Introduction

Delhi and its surrounding area (the National Capital Region, NCR) lies on an extension of the Peninsular shield, transverse to the Indo-Gangetic plains. The region is dominated by several tectonic features: Himalayan Main Boundary Thrust (MBT), Main Central Thrust (MCT), Delhi-Haridwar ridge, Delhi-Lahore ridge, Aravalli-Delhi fold, Sohna fault, Mathura fault, Rajasthan Great boundary fault, and Moradabad fault (Verma et al. 1995; Shukla et al. 2007; Prakash and Shrivastava 2012). Some of these features are shown in

✉ Brijesh K. Bansal
   bansal.moes@gmail.com; bkbansal@civil.iitd.ac.in

1 National Centre for Seismology, Ministry of Earth Sciences, New Delhi, India

2 Indian Institute of Technology Delhi, New Delhi, India

3 Universidad Nacional Autónoma de México, Mexico City, Mexico

Fig. 1. As a consequence, the NCR is exposed to seismic hazards from large and great earthquakes along the Himalayan arc, and small and moderate earthquakes at local and regional distances.

Historical seismicity in the NCR is plagued with uncertainty (see, e.g., Singh et al. 2013 for a summary). Catalogs based on instrumental recording list three significant earthquakes in and near NCR (Bansal et al. 2009). They occurred on 10 Oct 1956 near Bulandshahar, 27 Aug 1960 in Delhi, and 15 Aug 1966 near Moradabad. The 1960 Delhi earthquake is the largest, instrumentally-recorded event in the NCR. Hence, it has been one of the critical scenario earthquakes in the estimation of seismic hazard of the NCR. Yet the epicenter, depth, and magnitude of the earthquake are uncertain. The depth reported in different catalogs varies between 58 and 109 km and the magnitude between 5.3 and 6.0. From an exhaustive analysis of the event, Singh et al. (2013) concluded that it was shallow (depth $\leq$ 30 km but most likely $\leq$ 15 km) and its magnitude was M_w 4.8 (range M_w 4.6–4.9). A more reliable epicenter, as compared to the instrumentally-determined one, is provided by the area of the strongest seismic intensity: 28.47°N, 77.00°E (between Delhi Cantonment and Gurgaon). Quite possibly, the maximum magnitude in the NCR in the last 100 years has not exceeded 5.0.

Abundant low-level seismicity and the awareness of earthquake exposure of NCR has led to a steady increase in the seismic and accelerographic instrumentation in and near NCR during last two decades (Bhattacharya and Dattatrayam 2000; Kumar and Mittal
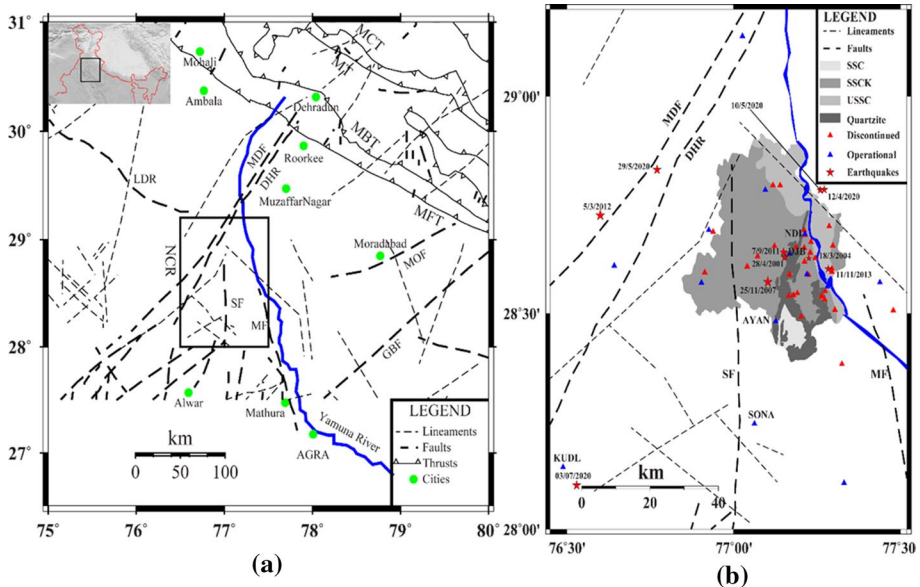
Fig. 1 **a** Structural features of Delhi and the surrounding region. *MFT*, *MBT*, *MCT* Main frontal thrust, Main boundary thrust, and Main central thrust, respectively. *DHR* Delhi-Haridwar ridge; *MDF* Mahendra-garh-Dehradun fault; *GBF* great boundary fault; *MOF* Moradabad fault; *MF* Mathura fault; *SF* Sohna fault. **b** An enlarged map of the rectangular area shown in the Fig. 1a. Surface geology, faults, and lineaments in Delhi and its vicinity. Stars: epicenters of the earthquakes analyzed in this study. Blue triangles: stations currently in operation; stations located on hard sites (NDI, DJB, AYAN, KUDL) are identified by name. Red triangles: discontinued stations. *SSC* Sand, silt, and clay; *SSCK* sand, silt, and clay with kankar; *USSC* Unoxidized sand, silt, and clay

2018; Shukla et al. 2018; Bansal et al. 2021a). Consequently, our knowledge of the seismicity of the region has improved, revealing a prolific activity of small earthquakes. The seismicity, at least at a small magnitude level, is diffused (Pandey et al. 2020). For this reason, it is not possible to relate events with specific tectonic features; rather the seismicity suggests an active source volume. This may be real or due to an error in the locations since the network is still sparse. Bansal et al. (2021b) made an effort to constrain the causative fault of the recent seismicity (April–May 2020) using morphotectonic analysis, Coulomb's failure stress changes, and fault plane solutions and inferred a new hidden fault.

The improved seismic network in and near NCR has produced high-quality recordings which permits source and ground motion studies of some of the NCR earthquakes. Source parameters and analysis of ground motion have been reported previously for the earthquakes of 28 April 2001 (M_w 3.3), 18 March 2004 (M_w 2.7), and 25 Nov 2007 (M_w 4.2) (Bansal et al. 2009; Singh et al. 2010) (Table 1). A preliminary analysis of the earthquake of 5 March 2012 (M_w 4.5) was presented by Bansal and Verma (2012). Recordings of Delhi and some Himalayan-arc earthquakes have been used to estimate seismic-wave amplification at several sites in the NCR with respect to the reference hard site of Ridge Observatory (station NDI) (Singh et al. 2002, 2010; Bansal et al. 2009; Mittal et al. 2013a, b).

An earthquake sequence began in the NCR on 12 April 2020 with an M_w 3.3 event. It was followed by earthquakes on 10 May 2020 (M_w 3.3), 29 May 2020 (M_w 4.0), and 3 July (M_w 3.9). These earthquakes were strongly felt in the NCR region and caused panic among the public. Regional moment tensor inversion and source spectrum of the 12 April earthquake as well as an analysis of the ground motion is presented by Pandey et al. (2020). The 12 April and 10 May events were nearly collocated. With respect to the earthquake of 12 April, the earthquake of 29 May occurred about 50 km to the west while that of 3 July was

Table 1 Source parameters of 10 well-recorded earthquakes in and near Delhi, the national capital region, analyzed in this study

Date	hr:min:sec	Lat °N	Long °E	Depth km	M_0 N-m	M_w	$\Delta\sigma$ MPa
28 Apr 2001	03:06:28.0	28.629	77.153	14.6	1.1×10^{14}	3.3	3.0
	03:06:25	28.588	76.841	10		3.7 (mb)	
18 Mar 2004	07:52:33.2	28.627	77.226	7.9	1.4×10^{13}	2.7	10.0
25 Nov 2007	23:12:20.3	28.572	77.103	29.6	2.1×10^{15}	4.2	13.0
	23:12:17	28.555	77.057	10		4.7 (mb)	
7 Sep 2011	17:58:19.2	28.641	77.150	10.5	2.24×10^{14}	3.5	4.9
	17:58:18	28.724	77.189	10		4.3 (mb)	
5 Mar 2012	07:41:04.6	28.726	76.601	15.0	6.2×10^{15}	4.5	2.6
	07:41:04	28.809	76.649	10		5.1 (mb)	
11 Nov 2013	20:11:34.2	28.602	77.284	13.0	4.8×10^{13}	3.1	3.1
12 Apr 2020	12:15:02.9	28.785	77.272	7.0	1.0×10^{14}	3.3	5.6
	12:15:02	28.832	77.361	10		3.8 (mb)	
10 May 2020	08:15:29.5	28.784	77.260	13.1	1.0×10^{14}	3.3	0.9
	08:15:27	28.727	77.352	10		3.7 (mb)	
29 May 2020	15:38:40	28.831	76.771	15.0	1.32×10^{15}	4.0	6.6
	15:38:46	29.225	77.092	57.1		4.2 (mb)	
03 July 2020	13:30:48	28.102	76.530	16.5	8.8×10^{14}	3.9	11.2
	13:30:47	28.078	76.536	32.8		4.4 (mb)	

Location and body-wave magnitude, m_b, if available in the NEIC, U.S. geological survey catalog are also listed

located about 105 km to the southwest (Fig. 1). A seismotectonic framework interpreting the NCR events is given by Bansal et al. (2021c). Recently, Tiwari et al. (2021) proposed that infrequent low magnitude earthquakes occurring in and around Delhi show a significant variation at annual seasonal scale and are correlated with the groundwater pumping for the irrigation, urban activities, and seasonally controlled hydrological loading cycle of freshwater aquifers.

The main objective of this study is to develop parameters needed to estimate ground motion in the NCR from postulated earthquakes applying the stochastic method (Boore 1983, 2003). This effort is critical for reliable estimation of seismic hazard in the region. Towards this objective, we analyze recordings of seven NCR earthquakes since 2011, including four that occurred during the 2020 sequence (Table 1). For each event, we estimate source spectrum, stress drop, and site amplification with respect to the reference hard site of NDI. The results from these seven earthquakes, along with those previously reported for the three other events, are used to develop the needed parameters for the prediction of ground motion. Amplification is estimated at 38 soft sites in the NCR using the recordings of the 10 earthquakes applying the standard spectral ratio (SSR) technique, accounting appropriately for the geometrical spreading. From the estimated site effects, we present median soft-site amplification of seismic waves. Thus, the ground motion from a postulated NCR earthquake may be estimated at any hard site and each of the 38 soft sites or a generic soft site. Alternately, real-time recording of an earthquake (located in/near NCR or in the Himalayan arc) at the reference site of NDI, along with the catalog of the site effects, may be used to estimate the ground motions at all other sites in near-real-time, valuable information for civil protection authorities.

A brief description of the earthquakes is given first, followed by the common methodology used in processing and analysis of the data of all events. For consistency, some of the source parameters of the three previous events are re-analyzed using this common methodology.

2 Earthquakes in National Capital Region

Earthquakes of 2001, 2004, and 2007 are discussed in Bansal et al. (2009) and Singh et al. (2010). Here we give brief description of the more recent events analyzed in this study.

2.1 7 September 2011 earthquake

The epicenter of the earthquake reported by the National Centre for Seismology (NCS) is in the heart of Delhi, about 8 km to the SW of Ridge Observatory (Table 1, Fig. 1). The NEIC epicenter (Table 1) is about 10 km N23°E of the NCR epicenter.

2.2 5 March 2012 Rohtak earthquake

This is one of the more significant events to occur in and near Delhi in recent years. It was located about 60 km to the west of Ridge Observatory, near the town of Rohtak. The epicenter of the earthquake falls near Mahendragarh- Dehradun fault (MDF) (Fig. 1). The earthquake was felt in Rohtak, Gurgaon, Delhi, Faridabad, and as far as Jaipur. A preliminary report on the event was published by Bansal and Verma (2012). Recordings of the event were used by

Mittal et al. (2013b) to study site effect. As it is one of the larger, well-recorded earthquakes in/near Delhi, it merits a detailed analysis.

2.3 11 November 2013 earthquake

A swarm-like earthquake activity occurred in Delhi on 11 Nov 2013. The sequence was widely felt in the city. Here we analyze the largest event of the sequence. It was located about 5 km NE of the offices of NCS located in the India Meteorological Department campus at Lodhi Road.

2.4 Earthquakes of 12 April and 10 May 2020

The earthquake of 12 April 2020 (M_w 3.3), with its epicenter located 12 km N30°E of Ridge Observatory, was felt as far south as Faridabad, a distance of about 35 km. It caused panic in the city although no damage was reported. According to U.S. Geological Survey Community Internet Intensity Map, which was based on 245 responses, the felt area extended ~35 km south of the NCS epicenter (Table 1). This small magnitude earthquake was felt by a relatively large number of persons considering perhaps because it occurred in the locked-down period of the Covid-19 pandemic when most people were indoors (Pandey et al. 2020; Singh 2020). The earthquake of 10 May occurred near the 12 April hypocenter and had almost the same magnitude. Yet only four responses are reported in the U.S. Geological Survey Community Internet Map. As we show later, this earthquake was deficient in high-frequency radiation as compared to the 12 April earthquake.

2.5 29 May 2020 earthquake

The earthquake was located about 50 km to the west of Ridge Observatory, 20 km N55°E of the 5 March 2012 event. Curiously, the epicenter reported by NEIC, U.S. Geological Survey is 50 km N35°E of the NCS epicenter (Table 1). The depth reported by NEIC is 45 km as compared to 15 km by the NCS (Table 1). Because of the large difference between the two locations, we carefully relocated the event. The RMS residual as a function of depth has a sharp minimum (0.47 s) at a depth of 15 km. (S-P) time at the nearest station is 3.6 s. There are 4 stations with (S-P) ≤ 5.2 s. The NCS location is, clearly, more accurate than that reported by the NEIC.

2.6 3 July 2020 Alwar earthquake

The epicenter of the earthquake was near Alwar, 93 km SW of Ridge Observatory (Fig. 1). As the (S-P) time at the closest station KUDL is 2.3 s, it follows that the depth of the event was less than 20 km. This is consistent with $H = 16.5$ km reported by NCS, not with 32.8 km given by NEIC, U. S. Geological Survey (Table 1).

3 Processing and analysis of data

Our analysis extensively uses the Fourier acceleration amplitude spectrum of the *S*-wave group. The time window chosen for the spectral analysis brackets 95% of the energy on the horizontal components of accelerograms beginning with the arrival of the *S*-wave. (In some cases, acceleration was computed by differentiating broadband velocity seismograms.) A 5% cosine taper is applied before computing the spectrum which is then smoothed by a 1/6 octave filter. Henceforth, we denote the geometric mean of the amplitude spectra of the two horizontal components as $A(f, R)$.

Under far-field, point-source approximation, $A(f, R)$ of an event at a distance R may be written as (see, e.g., Singh et al. 1999 for details):

$$A(f, R) = C \cdot G(R) \left[\left\{ f^2 \dot{M}_0(f) \right\} Site(f) e^{-\pi \kappa f} B(f) \right] \left[e^{-\pi p f R / \beta Q(f)} \right] \tag{1}$$

where

$$C = FPR_{qj}(2p)^2 / (4prb^3) \tag{2}$$

In equations above, $\dot{M}_0(f)$ is the moment rate spectrum so that $\dot{M}_0(f) \rightarrow M_0$ (the seismic moment) as $f \rightarrow 0$, R = hypocentral distance, $R_{\theta\phi}$ = average radiation pattern (0.55), F = free surface amplification (2.0), P takes into account the partitioning of energy in the two horizontal components $(1/\sqrt{2})$, β = shear-wave velocity at the source, ρ = density in the focal region, and $Q(f)$ = quality factor, which includes both anelastic absorption and scattering. The attenuation in the near-surface layer and the finite bandwidth of the observed spectrum imposed by the sampling rate are accounted by the parameter κ (Singh et al. 1982; Anderson and Hough 1984) and/or the Butterworth filter, $B(f)$. Often either κ or $B(f)$ is sufficient to explain the high-frequency falloff of the spectrum. Following Boore (1983), we take $B(f) = \left(1.0 + (f/fm)^{(8)}\right)^{(-0.5)}$. For the NCR earthquakes analyzed here, $B(f)$ with $f_m = 35$ Hz suffices. $Site(f)$ in Eq. (1) is the local site effect which we will take as 1 for hard sites in the NCR. The geometrical spreading term, $G(R)$, in Eq. (1) is taken as $1/R$ for $R \leq 100$ km and $1/(100R)^{0.5}$ for $R > 100$ km.

Similar to our previous studies of the NCR events, we take $Q(f) = 253 f^{0.80}$ which was estimated for the Himalayan arc region (Singh et al. 2004). $Q(f)$ has been estimated for the NCR region using coda waves (Mohanty et al. 2009; Das et al. 2018) and *S* waves (Sharma et al. 2015; Banerjee and Kumar 2018). As discussed later, reasonable choices of $Q(f)$ have a minor effect on the results. For the deeper earthquake of 2007 ($H = 30$ km; Table 1), β and ρ in the source region are taken as 4.2 km/s and 3.2 gm/cm³, respectively; for all other events the corresponding values are taken as 3.55 km/s and 2.85 gm/cm³. We take the logarithm of Eq. (1) and compute $\log \left[\dot{M}_0(f) Site(f) \right]$. Hard- and soft-site recordings are processed separately. For each event, we show plots of $\dot{M}_0(f)$ from hard sites and $\left[\dot{M}_0(f) Site(f) \right]$ from soft sites. We interpret the hard-site spectrum by the ω^2-source model of Brune (1970), $\dot{M}_0(f) = M_0 f_c^2 / \left(f^2 + f_c^2 \right)$, and obtain an estimation of the seismic moment (M_0) and corner frequency (f_c). The stress drop, $\Delta\sigma$, is related to M_0 and f_c by (Brune 1970): $\Delta\sigma = 8.47 M_0 \left(f_c / \beta \right)^3$.

M_0 and $\Delta\sigma$ of the earthquakes of 2001, 2004, and 2007 are given in Bansal et al. (2009) and Singh et al. (2010). They are listed in Table 1. Note that some of the values given in the table differ slightly from those reported in the original publications. This is because of uniform values of β and ρ used here.

4 Moment rate spectra and stress drops

$\dot{M}_0(f)$ and $[\dot{M}_0(f)\ Site(f)]$ of the earthquakes are shown in Fig. 2a–g. Both geometric mean and $\pm$ one standard deviation curves are presented. The panels identify hard and soft sites whose recordings were used in the computation. Most of the recordings were accelerograms. Seismic instrumentation in the NCR had undergone changes when the 2020 events occurred. For these events, the ground motion was recorded by both an accelerograph (100 samples/s) as well as a broadband seismograph (40 samples/s). Because the low-frequency signal is poorly resolved on accelerograms, for the 2020 events we patched $\dot{M}_0(f)$ and $\left[\dot{M}_0(f)Site(f)\right]$ constructed using the two datasets.
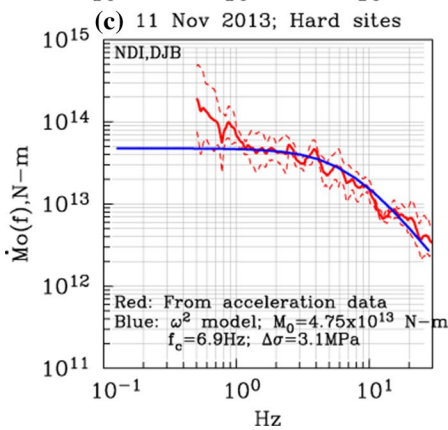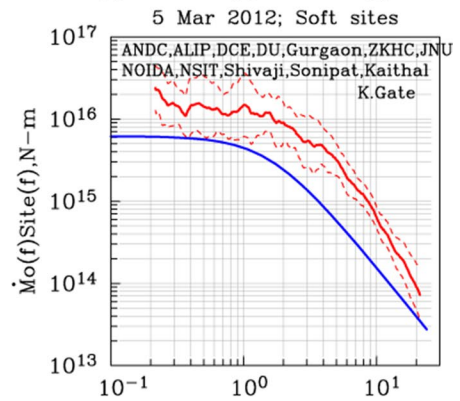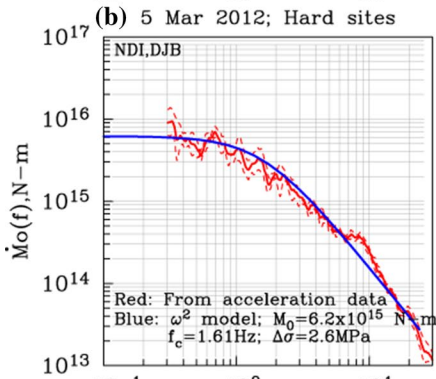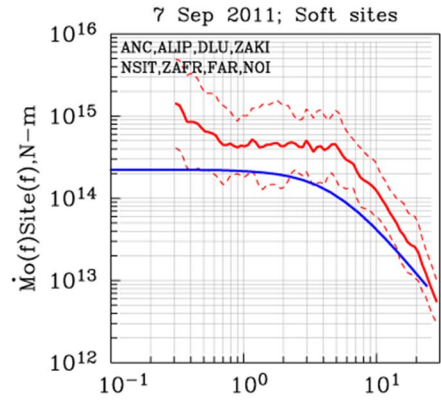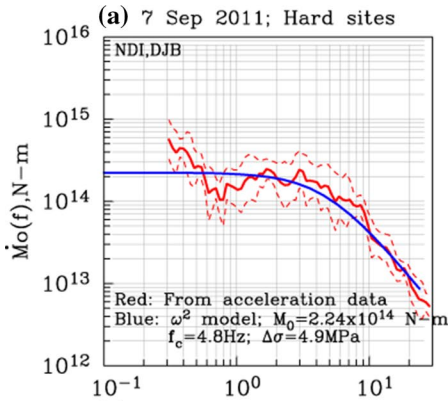
A Brune ω^2-source model was adjusted to $\dot{M}_0(f)$ by requiring that the theoretical curve simultaneously fit the observed spectrum both at low frequencies and high frequencies in the least-square sense. The selection of the low- and high-frequency band chosen for least-square fit was subjective. Theoretical curves are shown in blue in Fig. 2. Each $\dot{M}_0(f)$ panel gives corner frequency, f_c, and the stress drop, $\Delta\sigma$. The corresponding right panel illustrates $[\dot{M}_0(f)\ Site(f)]$. Superimposed on the plot is the theoretical curve for the ω^2-source model (shown in blue). The disparity between the blue curve and the geometric mean curve (shown in bold red) is a measure mean site effect.

From an examination of Fig. 2 we conclude that ω^2-source model is a fairly good approximation to the observed moment rate spectra of earthquakes in and near the NCR. If we exclude the 10 May 2020 event, then $\Delta\sigma$ ranges between 2.5 and 13 MPa, the average being 6 MPa. This is a fairly small range in view of the difficulty in reliable determination of f_c and cubic dependence of $\Delta\sigma$ on f_c, $\Delta\sigma \ \alpha \ M_0 \ (f_c/\beta)^3$.
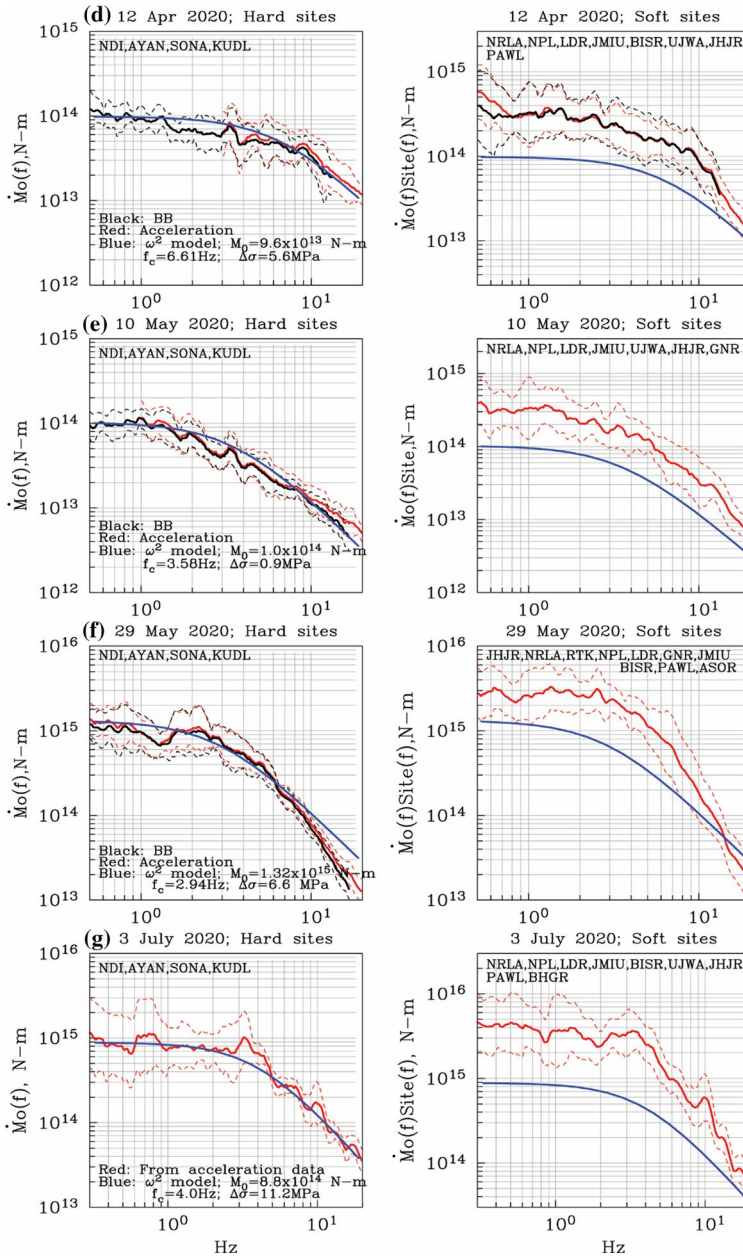
$\Delta\sigma$ of the 10 May 2020 earthquake (0.9 MPa) is much smaller than that of the nearby 12 April 2020 event (5.6 MPa). This agrees with the relatively small number of felt reports for the 10 May event. We envision that a patch of higher strength on the fault surface broke during the 12 April event, loading an adjacent patch of lower strength that, eventually, broke on 10 May. Next, we provide further evidence that the two events were collocated, had similar focal mechanism and M_w but the 10 May event was deficient in high-frequency radiation.

## 5 Deficient high-frequency radiation during 10 May 2021 earthquake

The displacement seismograms of the 12 April and 10 May 2020 events are compared at stations NRLA and NDI in Fig. 3. Amplitudes and waveforms at NRLA and NDI differ because of focal mechanism effect and difference in the site response. However, the seismograms are nearly identical during the two events at the same site, confirming that they were nearly collocated, and had similar magnitude and focal mechanism. We checked whether the high-frequency radiation was deficient ($\Delta\sigma$ was low) during the 10 May earthquake by computing spectral ratios of ground motion at each station during the two events. 12 April/10 May spectral ratios for the vertical component are shown in the bottom part of the figure. Around 1 Hz, the geometric mean ratio is ~1, implying the same seismic moment of both events. The ratio increases to 3 at 10 Hz and then decreases reaching 2 at 40 Hz. The figure demonstrates that the 10 May event was deficient at high frequencies as compared to the event of 12 April. We expect, and later

(a) 7 Sep 2011; Hard sites — NDI,DJB. Red: From acceleration data. Blue: ω^2 model; $M_0=2.24\times10^{14}$ N-m; $f_c=4.8$Hz; $\Delta\sigma=4.9$MPa

7 Sep 2011; Soft sites — ANC,ALIP,DLU,ZAKI NSIT,ZAFR,FAR,NOI

(b) 5 Mar 2012; Hard sites — NDI,DJB. Red: From acceleration data. Blue: ω^2 model; $M_0=6.2\times10^{15}$ N-m; $f_c=1.61$Hz; $\Delta\sigma=2.6$MPa

5 Mar 2012; Soft sites — ANDC,ALIP,DCE,DU,Gurgaon,ZKHC,JNU NOIDA,NSIT,Shivaji,Sonipat,Kaithal K.Gate

(c) 11 Nov 2013; Hard sites — NDI,DJB. Red: From acceleration data. Blue: ω^2 model; $M_0=4.75\times10^{13}$ N-m; $f_c=6.9$Hz; $\Delta\sigma=3.1$MPa

11 Nov 2013; Soft sites — GGI,VCD,ZKC,DLU,JNU NTPC,RDG,IGN,DCE,NSIT,ALIP

Fig. 2 (Left panels) Moment rate spectrum, $\dot{M}_0(f)$, computed from recordings at hard sites (named in the upper left corner). Geometric mean and $\pm$ one standard deviation curves are shown. Fit to the spectrum by a Brune ω^2-source model (blue curve) gives seismic moment, M_0, and corner frequency, f_c (and hence stress drop, $\Delta\sigma$). These values are listed in the panels. (Right panels) $\left[\dot{M}_0(f)Site(f)\right]$, computed from recordings at soft sites (named in the upper part of the frame). Superimposed on this plot is the theoretical curve for the ω^2-source model (blue curve). The disparity between the blue curve and the geometric mean curve (shown in bold red) is a measure mean site effect
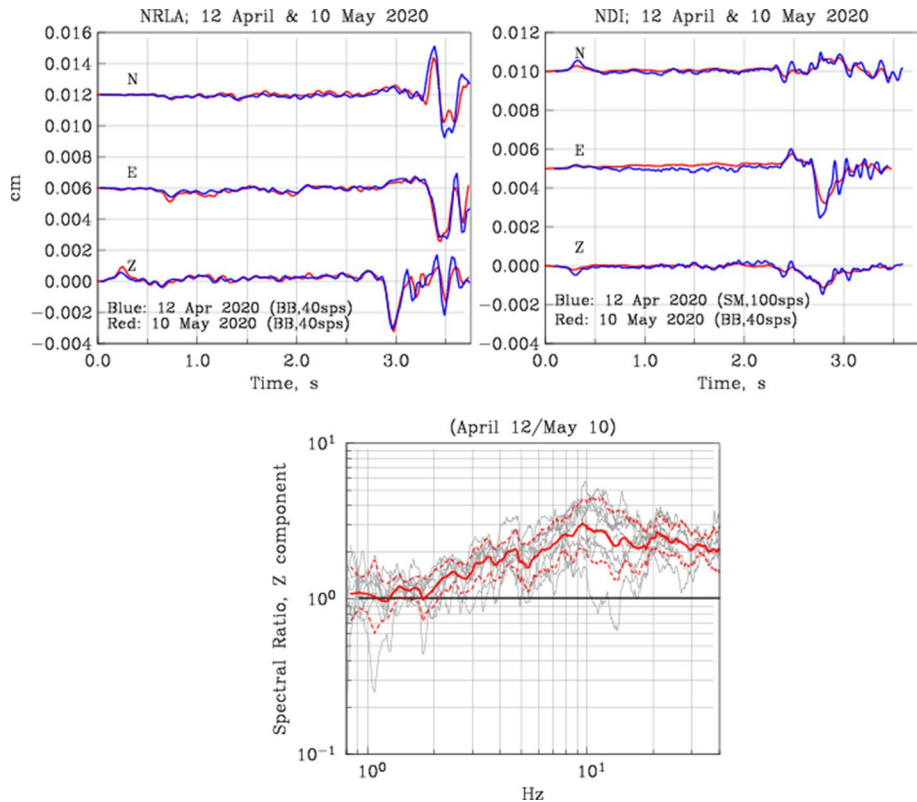
Fig. 3 (Top) Displacement seismograms of 12 April and 10 May 2020 earthquakes at NRLA (left) and NDI (right). Traces suggest that the two events were nearly collocated, and had same magnitude and focal mechanism. (Bottom) (12 April/10 May) spectral ratios. Red continuous curve: geometrical mean of the ratios. Ratio shows that 10 May event was deficient at higher frequencies compared with 12 April earthquake

confirm, higher peak ground acceleration and velocity (PGA and PGV) during the 12 April earthquake as compared to the 10 May event.

6 Site effect in the NCR

Site effect in the NCR is clearly seen in the plots of $\dot{M}_0(f)$ and $\left[\dot{M}_0(f)Site(f)\right]$ presented in Fig. 2. The amplification and variability of ground motion at soft sites can be appreciated in the plots of Fourier acceleration spectra during the 11 Nov 2013 earthquake (Fig. 4). This event was recorded at two hard sites (NDI and DJB) and eight soft sites within a hypocentral distance range of 14.4–19.1 km. Since the distances are roughly equal, the spectra, in the absence of site effect, should be similar. However, as Fig. 4 illustrates, they are highly variable at soft sites and are consistently higher than those at the hard sites.

Because of its importance in seismic hazard estimation, the site effect in Delhi has been studied through numerical modeling (Parvez et al. 2004), microtremor recordings (Mukhopadhyay et al. 2002), borehole data (Iyengar and Ghosh 2004), and earthquake recordings (Singh et al. 2002, 2010; Bansal et al. 2009; Mittal et al. 2013a, b). The
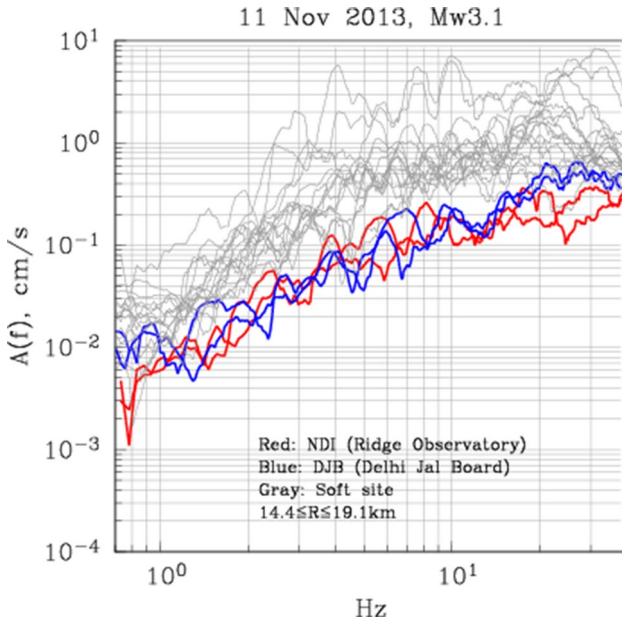
Fig. 4 Fourier acceleration spectra of 11 Nov 2013 earthquake at two hard sites (NDI and DJB) and eight soft sites located within hypocentral distance range of 14.4–19.1 km. The spectra at soft sites are highly variable and, as expected, are consistently higher than those at the hard sites

estimation of site effect in Delhi using earthquake recordings is based on the application of the standard spectral ratio (SSR) technique. In this technique, the spectral amplification at the site of interest is measured with respect to a reference, hard site. For the NCR the station NDI (Ridge Observatory) is an ideal reference site as it is the oldest seismic station in Delhi that remains in operation. Most of the events recorded at other sites in Delhi are also recorded at NDI. (All events analyzed here were recorded at NDI). Since a large dataset is available at NDI, it is possible to predict ground motion from postulated earthquakes at this site. If ground motion at NDI is known (either recorded or predicted), then it can be computed at all other sites with known SSRs through the application of the stochastic method.

SSR technique is based on the assumption that the source is sufficiently far as compared to the distance between the sites so that the expected ground motion, in the absence of site effect, is the same at the two sites. This assumption may not be valid for local events. Yet, site effect studies in Delhi using the SSR technique have ignored this issue. As the hypocentral distances to NDI and stations at soft sites differ, in this study, we reduce the S-wave spectrum of each of the two horizontal components at NDI to the distance of the station of interest by taking $Q(f) = 253f^{0.8}$ and geometrical spreading of $1/R$ (R is ≤ 100 km for all stations). The ratio of the geometric mean of the observed horizontal spectra at the station to the geometric mean of the reduced spectra provides the SSR. Note that in this modification of the SSR technique we are ignoring possible focal mechanism, path, and directivity effects.

We analyzed 74 accelerograms produced by the 10 earthquakes listed in Table 1. These accelerograms were recorded at 38 sites. In Fig. 5, we show examples of SSRs at six sites where three or more earthquakes were recorded. We note that SSRs at the same site are
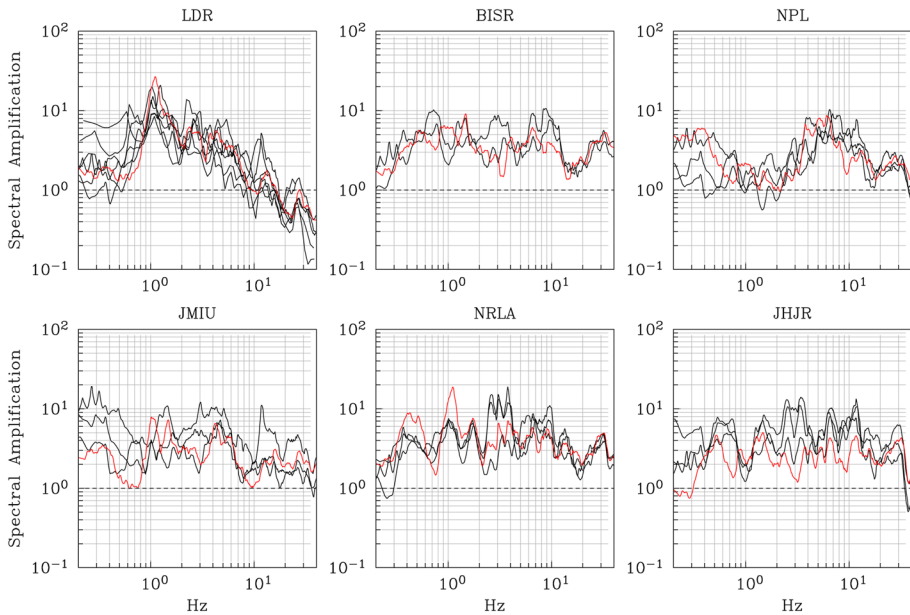
Fig. 5 Examples of spectral amplification at six sites with respect to the reference hard site of NDI (Ridge Observatory) estimated using a modified SSR technique. Three or more earthquakes were recorded at these sites. The red curve corresponds to the 3 July 2020 earthquake

reasonably similar at frequencies above about 0.8 Hz; below 0.8 Hz the SSR, in some cases, is affected by noise and is not reliable.

Spectral amplification at a given soft site is critical in the estimation of site-specific ground motion. Here, however, we will be concerned with the prediction of ground motion at generic hard and soft sites in Delhi; for this purpose, we derive a mean site effect in the NCR. In Fig. 6 we show SSRs computed for the seven earthquake since 2011 (Table 1). For each earthquake the geometric mean and ± one standard deviation SSR curves are given. The mean curves slightly differ, partly because the sites where the events were recorded were not the same. In the last panel of the figure, we have merged SSRs of these seven events with those from the earlier three earthquakes (Table 1). The geometric mean curve of SSRs of all 10 events is shown in the last panel. This curve is the mean spectral amplification at soft sites in NCR. It may be approximated by a constant SSR of 3.5 in the frequency range 0.25–10 Hz.

# 7 Observed and predicted ground motions from earthquakes in the NCR

7.1 Observed data

As mentioned before, ground motions recorded during the 2001, 2004, and 2007 earthquakes were analyzed in previous studies (Bansal et al. 2009; Singh et al. 2010). Here
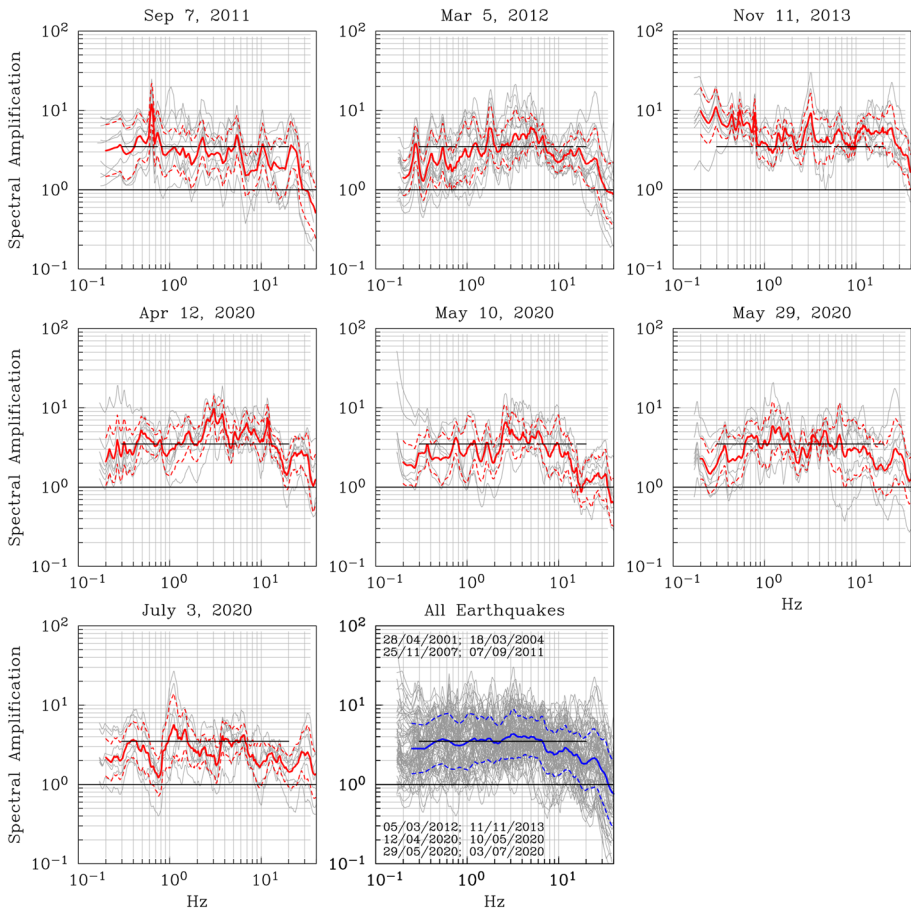
Fig. 6 Spectral amplification with respect to the reference hard site of NDI computed for earthquakes of 2011, 2012, and 2013, and four earthquakes of the 2020 sequence. For each earthquake, geometric mean and ± one standard deviation curves are given. In the last panel, the spectral ratios of these seven events are merged with those from the three earlier earthquakes. The geometric mean of spectral amplification at soft sites in NCR and ± one standard deviation curves of the 10 events are shown in this panel. The mean amplification curve may be approximated by a constant value of 3.5 in the frequency range 0.25–10 Hz

we include data from the earthquakes of 2011, 2012, 2013, and the four events of the 2020 sequence to those of the previous three events for a more comprehensive ground motion study. Plots of peak horizontal ground acceleration (PGA) and velocity (PGV) as a function of distance R of the ten events ($2.6 \leq M_w \leq 4.5$) is shown in Fig. 7. Hard- and soft-site data are identified by solid and open circles, respectively. Sites in/near NCR which we have classified as hard are NDI, DJB, SONA, AYAN, and KUDL. For some events, we have added data from stations of regional broadband networks, located at $R \leq 300$ km. As expected from the previous discussion, PGA and PGV values from the 12 April 2020 earthquake are significantly higher than those from the 10 May 2020 event even though the two earthquakes had the same magnitude.
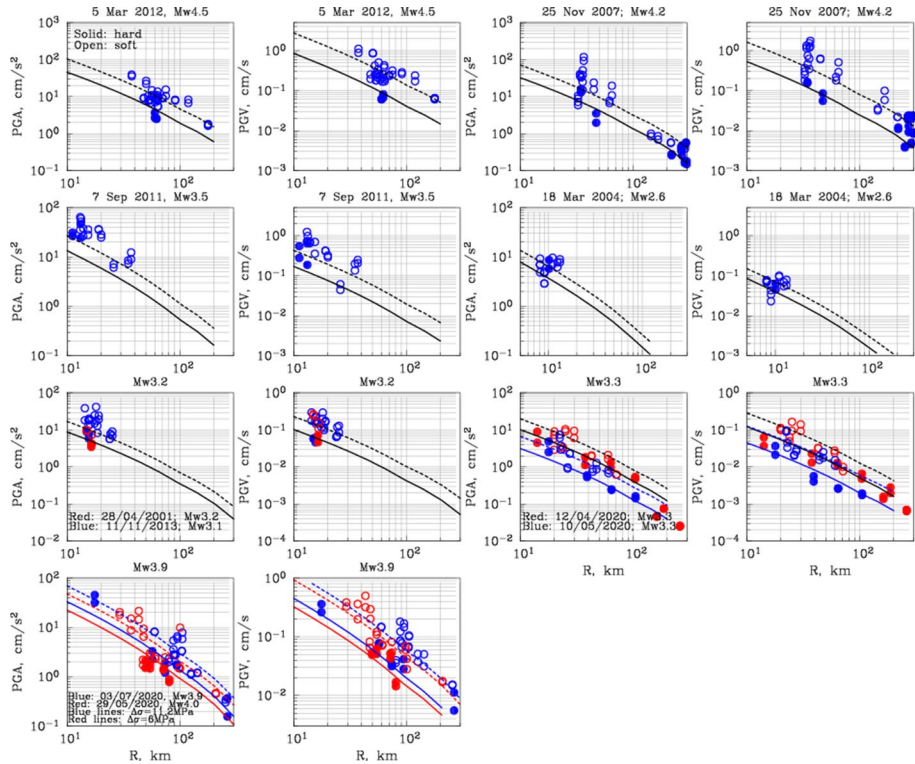
Fig. 7 Observed peak horizontal ground acceleration (PGA) and velocity (PGV) as a function of distance, *R*, of the 10 events analyzed in this study. Note that PGA and PGV values from the 12 April 2020 earthquake are significantly higher than those from the 10 May 2020 event even though the two earthquakes were collocated and had the same magnitude. For each event, the predicted PGA and PGV curves, based on the stochastic method assuming a Brune ω^2- source model with $\Delta\sigma = 6$ MPa, are superimposed on the data. For earthquakes of 10 May and 3 July 2020 the predictions with $\Delta\sigma$ of 0.9 and 11.2 MPa, respectively, also shown in the figure, better fit the data

7.2 Parameters needed for the application of the stochastic method

We refrain from developing a ground motion prediction equation (GMPE) from the available sparse dataset. Instead, we seek parameters that, in conjunction with the stochastic method (Boore 1983, 2003), may be used to estimate ground motion from future earthquakes. The method requires an estimation of the Fourier spectrum of the ground motion at the site of interest. Here we compute the spectrum using Eq. (1). We assume a Brune ω^2-source which is completely specified by M_0 and $\Delta\sigma$ of the event. We seek a generic $\Delta\sigma$, which along with $Q(f) = 253f^{0.80}$ and $f_m = 35$ Hz, would generate PGA and PGV in agreement with those observed during the NCR earthquakes (Fig. 7). This $\Delta\sigma$ may then be used in computing ground motions during postulated earthquakes. A parameter needed in the application of the stochastic method is the duration of the intense part of the ground motion, T_d, which we take as $T_d = \left(1/f_c\right) + 0.05R + 3.0$.

We first check whether the Brune ω^2-source model, with appropriate M_0 and $\Delta\sigma$ for the event (Table 1) and $Q(f) = 253f^{0.80}$ and $f_m = 35$ Hz, generates spectrum that agrees with the observed spectrum at the reference NDI site. We note that the accelerograms of the
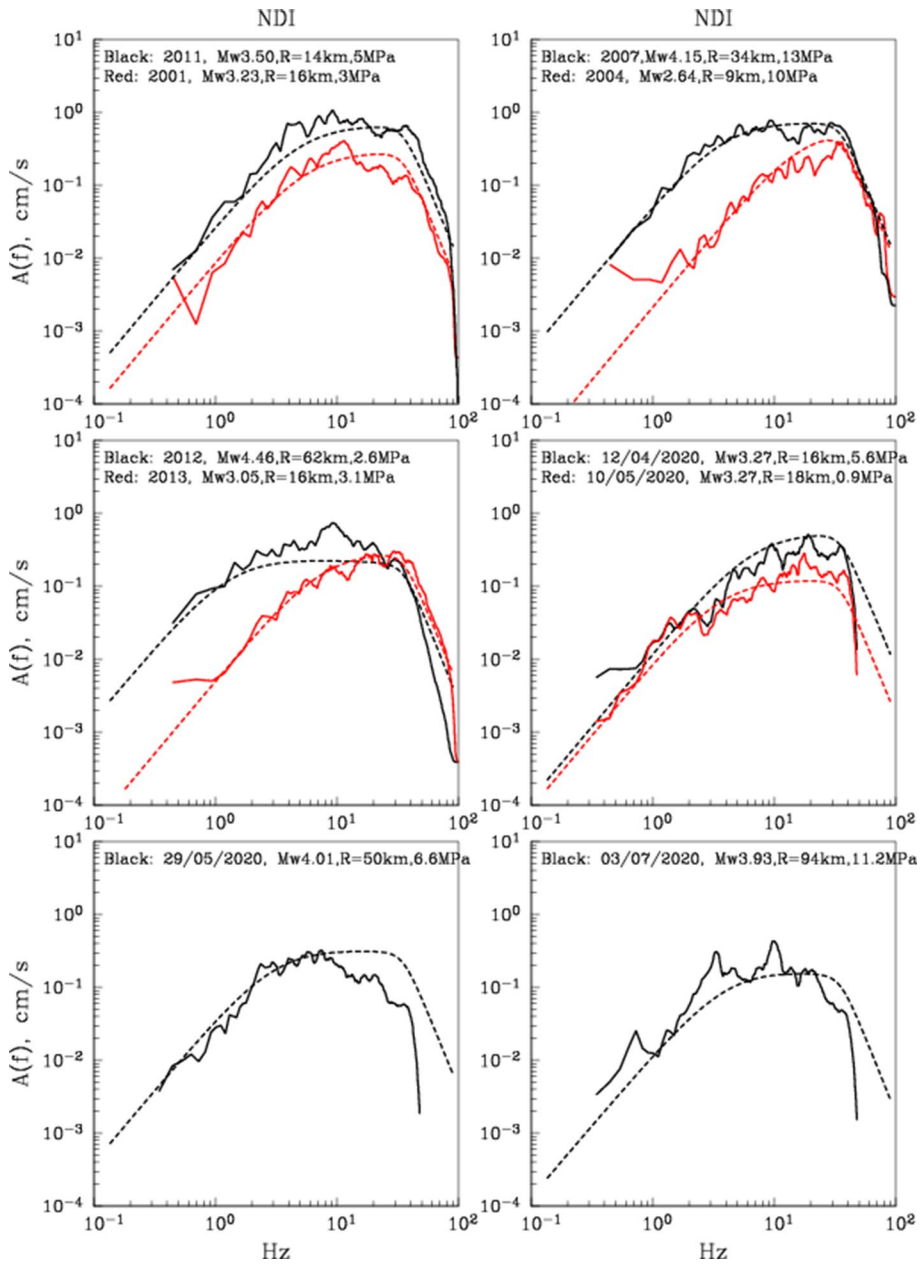
Fig. 8 Comparison of observed acceleration spectra (geometric mean of the two horizontal components) and predicted spectra at the reference hard site of NDI. Predictions are for a Brune ω^2- source model using Eq. 1. Other parameters needed in Eq. 1 are discussed in the text

events before 2020 and those recorded during the 2020 events at NDI were recorded at 200 and 100 sps, respectively. Thus, to facilitate the comparison, we low-pass filtered the NDI accelerograms at 35 Hz.

The geometric mean of *S*-wave acceleration spectra of the two horizontal components are shown in Fig. 8 along with the predicted spectra. The two spectra are reasonably similar. The difference in the spectra is greater if the stress drop has been estimated from more hard-site recordings than from NDI alone. Spectra of the 2020 events differ from the computed spectra at high frequencies ($f > 35$ Hz) because of the low Nyquist frequency (50 Hz).

7.3 Sensitivity of the results on the choice of *Q(f)*

As mentioned earlier, there are some studies which report *Q(f)* for the NCR region. To investigate the sensitivity of the results on the choice of *Q(f)*, we compared our predicted spectra at NDI with those from two extreme *Q(f)* relations for the NCR: $Q(f) = 162f^{0.835}$ (Banerjee and Kumar 2018) and $98f^{1.07}$ (Sharma et al. 2015). Figure 9 shows theoretical and observed spectra for the earthquakes of 2007 and 2012. Here theoretical spectra have been computed with $f_m = 35$ Hz and the same $\Delta\sigma$ which we found appropriate when *Q(f)* was taken as $253f^{0.8}$. We note that the theoretical predictions are indistinguishable if M_w is changed slightly (the values are given in the figure). Even in the case of large *R* (e.g., earthquake of 2012) and low $Q(f) = 98f^{1.07}$ the required change in M_w is only 0.1. We conclude that a reasonable choice of *Q(f)* has only a minor effect on the results.

7.4 Prediction of ground motion in NCR: stochastic method

To predict ground motions from postulated earthquakes, we take $\Delta\sigma$ of 6 MPa, the average value for the NCR events ignoring the anomalously low stress-drop earthquake of 10 May 2020 (Table 1). PGA and PGV curves as a function of *R* computed via the stochastic method with $\Delta\sigma = 6$ MPa are shown in Fig. 7 along with the observed PGA and PGV values. Computations performed excluding and including mean site effect are shown in the figure. Considering the large scatter in the observed data, the predicted curves with
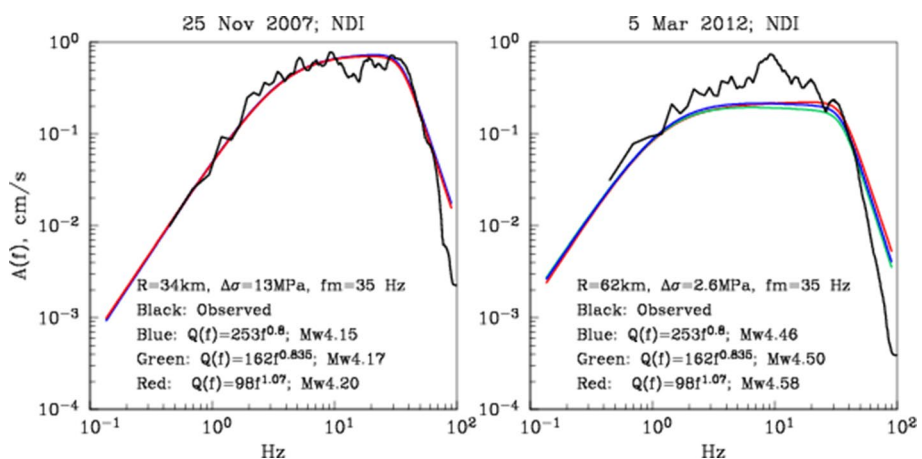
Fig. 9 Comparison of observed and predicted acceleration spectra at the reference hard site of NDI for the earthquakes of 2007 and 2012. Predicted spectra are shown for three *Q(f)* relations with fixed $\Delta\sigma$ and f_m. Note that the predictions are indistinguishable if M_w is changed slightly
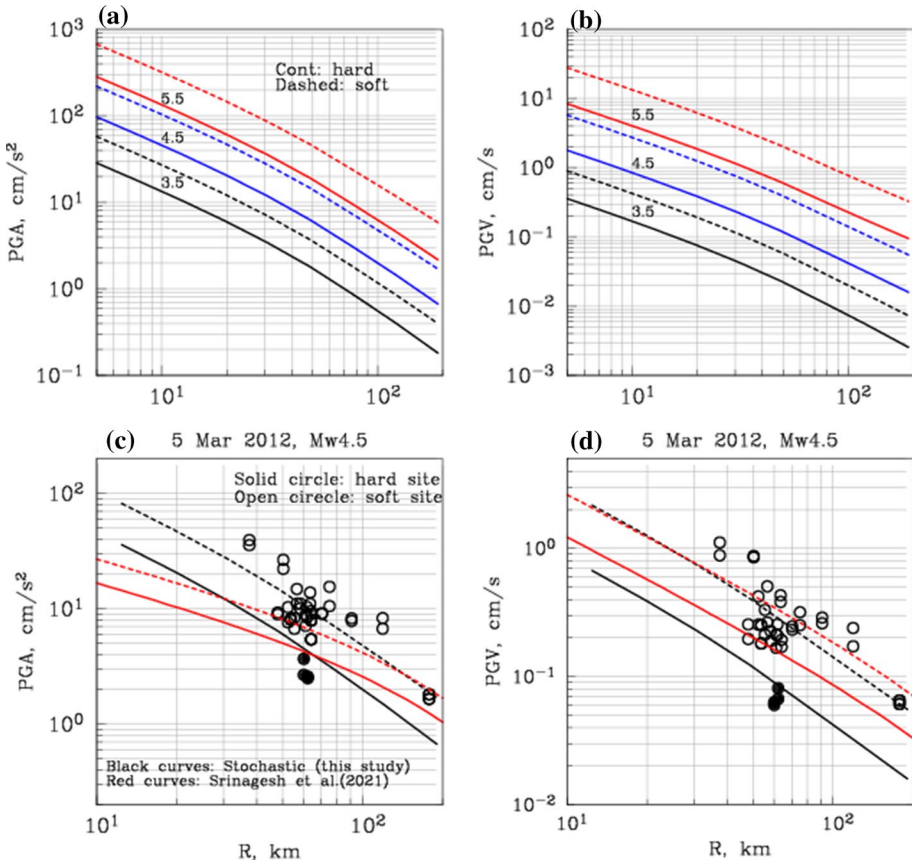
Fig. 10 **a** and **b** Predicted PGA and PGV curves at generic hard and soft sites in the NCR as a function of R for M_w 3.5, 4.5, and 5.5 earthquakes. Predictions are based on the stochastic method assuming a Brune ω^2-source with $\Delta\sigma = 6$ MPa. **c** Observed PGA during 5 March 2012 (M_w 4.5) earthquake along with predicted curves from the stochastic method (this study) and GMPE of Srinagesh et al. (2021) constructed from data of western Himalayan arc earthquakes. Predictions are shown for both hard (continuous) and soft sites (dashed). **d** Observed PGV during 5 March 2012 earthquake and predicted curves from the stochastic method and the GMPE of Srinagesh et al. (2021)

$\Delta\sigma = 6$ MPa work reasonably well. Once again, observed PGA and PGV values from the earthquake of 10 May 2020 (M_w 3.3) are exceptionally low; the predicted curves with $\Delta\sigma$ of 0.9 MPa fit the data well. We surmise that the ground motions in the NCR at typical hard and soft sites may be predicted using the stochastic method assuming a Brune ω^2-source model with $\Delta\sigma = 6$ MPa.

Predicted PGA and PGV curves at generic hard and soft sites in the NCR as a function of R for M_w 3.5, 4.5, and 5.5 earthquakes are illustrated in Fig. 10. We refrain from predicting ground motions during $M_w \geq 6$ earthquakes for two reasons. First, there is no evidence of the occurrence of an $M_w > 5$ event in the NCR in last 120 years. In fact, as mentioned in the introduction, there is strong evidence that the largest instrumentally recorded 1960 Delhi earthquake had a magnitude less than 5 (Singh et al. 2013). Second, simulation of $M_w \geq 6$ earthquake at short distances should include both finite-fault and near-field effects. This is not possible in our stochastic simulation which is based on point source, far-field

approximation. There are some studies which simulate ground motions for $M_w \geq 6$ earthquakes in the NCR (e.g., Mittal et al. 2016; Sandhu et al. 2020). These studies, however, do not account for the near-field effects.

7.5 Prediction of ground motion in NCR: stochastic method versus GMPE

Several GMPEs have been developed for Himalayan arc earthquakes (e.g., Singh et al. 1996; Sharma 1998; Iyengar and Ghosh 2004; Sharma et al. 2009). GMPE of Singh et al. (1996) is based on recordings of only 5 Himalayan earthquakes. Iyengar and Ghosh (2004) derived a GMPE which they utilized in their seismic hazard study of the NCR. A subset of the data employed by Iyengar and Ghosh had previously been used by Sharma (1998) in the derivation of a GMPE for PGA. Sharma et al. (2009) derived a GMPE merging data from the Himalayan and Zagros regions. Singh et al. (2010) found that the GMPEs of Iyengar and Ghosh (2004) and Sharma et al. (2009) greatly overestimate observed PGA in Delhi during the 25 Nov 2007 (M_w 4.1) earthquake. This was not surprising since the data used in the construction of these GMPEs came almost entirely from $M_w \geq 5.5$ earthquakes. Singh et al. (2010) reported that these GMPEs also overestimate PGA in the Delhi region from earthquakes originating in the Himalayas. They concluded that these GMPEs should neither be used to predict motions in the NCR from local $M_w < 5$ earthquakes nor from earthquakes originating in the Himalayan arc.

A new GMPE has been derived by Srinagesh et al. (2021) which is based on the recordings of 14 shallow western Himalayan arc earthquakes ($4.3 \leq M_w \leq 7.9$). As the data set includes seven earthquakes in M_w range 4.3–5.0, we explored the validity of this GMPE in predicting ground motions in the NCR from local earthquakes. In Fig. 9 (bottom two panels) observed PGA and PGV during the Rohtak earthquake of 5 March 2012 (M_w 4.5) are compared with the predictions from our stochastic simulation and the GMPE of Srinagesh et al. (2021). It is not surprising that the stochastic simulations fit the observed data better than the predictions from the GMPE of Srinagesh et al. which underestimates PGA at soft sites and overestimates it at hard sites. The same is true for PGV although the prediction at soft sites is only slightly underestimated. We surmise that attenuation relations developed for the Himalayan arc earthquakes may not appropriate for peak ground motions from earthquakes in the NCR. Stochastic simulations using parameters developed in this study are likely to provide more reliable ground motion estimations.

8 Discussion and conclusions

We have studied 10 well-recorded local earthquakes ($2.7 \leq M_w \leq 4.5$) in the NCR (including four that occurred in 2020) to retrieve their source parameters using hard-site recordings. All events have been analyzed using a uniform procedure. We find that spectra at hard sites are well-fit with a Brune ω^2-source model, $Q(f) = 253 f^{0.8}$, $f_m = 35$ Hz, and geometrical spreading of $1/R$ (Eq. 1). Other reasonable choices of $Q(f)$ have only a minor effect on the results because of relatively short hypocentral distances involved ($R < 100$ km). Based on these results, estimated site effects at soft sites, and analysis of recorded ground motions, we have developed parameters needed for the application of stochastic method to estimate of ground motions at typical hard and soft sites in the NCR during postulated earthquakes. Below we summarize the results.

1. The source spectra of nine out of 10 events require a stress drop between 3 and 13 MPa (average ~6 MPa) (Table 1). The exception is the earthquake of 10 May 2020 (M_w 3.3) which had a very low-stress drop, 0.9 MPa. This earthquake was located near the 12 April 2020 (M_w 3.3) event. Even though these two events had the same magnitude, the 10 May earthquake was significantly deficient in high-frequency radiation. As a consequence, observed PGA and PGV values were, relatively, low. Presumably, a patch of higher strength on the fault surface broke during the 12 April event, loading an adjacent patch of lower strength that, eventually, broke on 10 May.

2. Site effect has been estimated at 38 sites in the NCR using a modified Standard Spectral Ratio (SSR) technique, and taking NDI (Ridge Observatory) as the reference hard site. Only a few sites in the NCR have more than three recordings of earthquakes. The site effects at these sites during different earthquakes are fairly similar (Fig. 5). We also computed the geometric mean spectral amplification at soft sites. Thus, if the Fourier spectrum of an earthquake at NDI is known either from a recording or via a source model with appropriate attenuation parameters (Eq. 1) then the Fourier spectra can be estimated at each of the 38 soft sites or a generic soft site in the NCR. The earthquake may have its origin in the Himalayan arc or within NCR. These spectra can then be used to estimate ground motion parameters via the stochastic method. This is a powerful technique to produce near-realtime ground motion map for the NCR using only the NDI recording, thus providing extremely useful information for civil protection authorities. Such an approach is currently in use in Mexico City (Ordaz et al. 2017).

3. Fourier spectrum at NDI from a postulated earthquake in NCR may be estimated using a Brune ω^2-source model with a stress drop of 6 MPa, $\kappa = 0.0$ s, $Q(f) = 253 f^{0.80}$, and a cut-off frequency f_m of 35 Hz in Eq. 1. Figure 10 shows predicted PGA and PGV at generic hard and soft sites in the NCR from local and regional M_w 3.5, 4.5, and 5.5 earthquakes ($R < 100$ km). These predictions differ from those given by GMPEs which are based on recordings from earthquakes along the Himalayan arc. For example, observed PGA and PGV during the Rohtak earthquake of 5 March 2012 (M_w 4.5) are compared with the predictions of our stochastic simulation and the recently constructed GMPE by Srinagesh et al. (2021) in the bottom frames of Fig. 10. Even though the new GPME does better than others (not shown in the figure), it is clear that the attenuation relations constructed for the Himalayan arc earthquakes may not appropriate to predict ground motion from earthquakes in the NCR. Stochastic simulations using parameters developed in this study are likely to provide more reliable ground motion estimations.

4. Some studies have employed the empirical Green's function (EGF) technique to simulate ground motion in the NCR during larger events (Singh et al. 2002; Bansal et al. 2009; Mittal et al. 2015). EGF simulation has the advantage that the site and path effects are automatically included in the calculations. The method is not applicable if the locations of the postulated earthquake and the site of interest differ from the corresponding locations for the EGF event. Both methods assume that the point-source, the far-field approximation is valid. In the epicentral region, this approximation may be grossly violated for $M_w > 5.5$ earthquakes.

5. As mentioned earlier, there is no evidence of instrumentally recorded $M_w > 5$ events in the NCR in the last 120 years. Nevertheless, since there are many mapped faults and lineaments in the region, earthquakes with $M_w \geq 6$ can't be ruled out. For seismic hazard estimation, however, it is critical to establish the recurrence period of such events. Synthesis of ground motion from such earthquakes will also require due consideration of finite fault and near-field effects.

Data availability Data used in the present study are collected from the published sources (referred in MS) and presented in the text. The earthquake data are available from National Centre for Seismology and could be requested through the website (https://seismo.gov.in/).

Declarations

Conflict of interest The authors declare no conflict of interest.

References

Anderson JG, Hough SE (1984) A model for the shape of the Fourier amplitude spectrum of acceleration at high frequencies. Bull Seismol Soc Am 74:1969–1993

Banerjee S, Kumar A (2018) Determination of seismic wave attenuation in Delhi, India, towards quantification of regional seismic hazard. Nat Hazards 92(2):1039–1064. https://doi.org/10.1007/s11069-018-3238-7

Bansal BK, Verma M (2012) The M 4.9 Delhi earthquake of 5 March 2012. Curr Sci 102:1704–1708

Bansal BK, Singh SK, Dharmaraju R et al (2009) Source study of two small earthquakes of Delhi, India, and estimation of ground motion from future moderate, local events. J Seismol 13:89–105. https://doi.org/10.1007/s10950-008-9118-y

Bansal BK, Pandey AP, Singh AP, Suresh G, Singh RK, Gautam JL (2021a) National seismological network in India for real-time earthquake monitoring. Seismol Res Lett 20:1–15. https://doi.org/10.1785/0220200327

Bansal BK, Mohan K, Haq AU, Verma M, Prajapati SK, Bhat GM (2021b) Delineation of the causative fault of recent earthquakes (April-May 2020) in Delhi from seismological and morphometric analysis. Jour Geol Soc India 97:451–456

Bansal BK, Mohan K, Verma M, Sutar A (2021c) A holistic seismotectonic model of Delhi region. Nat Sci Rep 11:13818. https://doi.org/10.1038/s41598-021-93291-9

Bhattacharya SN, Dattatrayam RS (2000) Recent advances in seismic instrumentation and data interpretation in India. Curr Sci 79:1347–1358

Boore DM (1983) Stochastic simulation of high-frequency ground motions based on seismological models of the radiated spectra. Bull Seismol Soc Am 73:1865–1884

Boore DM (2003) Simulation of ground motion using the stochastic method. Pure Appl Geophys 160:635–676. https://doi.org/10.1007/PL00012553

Brune JN (1970) Tectonic stress and the spectra of seismic shear waves from earthquakes. J Geophys Res 75:4997–5009. https://doi.org/10.1029/jb075i026p04997

Das R, Mukhopadhyay S, Singh RK, Baidya PR (2018) Lapse time and frequency-dependent coda wave attenuation for Delhi and its surrounding regions. Tectonophysics 738:51–63

Iyengar RN, Ghosh S (2004) Microzonation of earthquake hazard in Greater Delhi area. Curr Sci 87:1193–1202

Kumar A, Mittal H (2018) Strong-motion instrumentation: current status and future scenario. Advances in Indian earthquake engineering and seismology: contributions in honour of Jai Krishna. Springer, Cham, pp 35–54

Mittal H, Kamal KA, Singh SK (2013a) Estimation of site effects in Delhi using standard spectral ratio. Soil Dyn Earthq Eng 50:53–61. https://doi.org/10.1016/j.soildyn.2013.03.004

Mittal H, Kumar A, Kumar A (2013) Site effects estimation in Delhi from the Indian strong motion instrumentation network. Seismol Res Lett 84:33–41. https://doi.org/10.1785/0220120058

Mittal H, Kumar A, Kumar A, Kumar R (2015) Analysis of ground motion in Delhi from earthquakes recorded by strong motion network. Arab J Geosci 8:2005–2017. https://doi.org/10.1007/s12517-014-1357-3

Mittal H, Wu YM, Chen DY, Chao WA (2016) Stochastic finite modeling of ground motion for March 5, 2012, Mw 4.6 earthquake and scenario greater magnitude earthquake in the proximity of Delhi. Nat Hazards 82(2):1123–1146

Mohanty WK, Prakash R, Suresh G, Shukla AK, Walling MY, Srivastava JP (2009) Estimation of coda wave attenuation for the national capital region, Delhi, India using local earthquakes. Pure Appl Geophys 166(3):429–449

Mukhopadhyay S, Pandey Y, Dharmaraju R et al (2002) Seismic microzonation of Delhi for ground-shaking site effects. Curr Sci 87:877–881

Ordaz M, Reinoso E, Jaimes MA, Alcántara L, Pérez C (2017) High-resolution early earthquake damage assessment system for Mexico City based on a single-station. Geofísica Internacional 56:117–135

Pandey AP, Suresh G, Singh AP et al (2020) A widely felt tremor (ML 3.5) of 12 April 2020 in and around NCT Delhi in the backdrop of prevailing COVID-19 pandemic lockdown: analysis and observations. Geomat Nat Hazards Risk 11:1638–1652. https://doi.org/10.1080/19475705.2020.1810785

Parvez IA, Vaccari F, Panza GF (2004) Site-specific microzonation study in Delhi metropolitan city by 2-D modelling of SH and P-SV waves. Pure Appl Geophys 161:1165–1185. https://doi.org/10.1007/s00024-003-2501-2

Prakash R, Shrivastava JP (2012) A review of the seismicity and seismotectonics of Delhi and adjoining areas. J Geol Soc India 79(6):603–617. https://doi.org/10.1007/s12594-012-0099-7

Sandhu M, Sharma B, Mittal H, Yadav RB, Kumar D, Teotia SS (2020) Simulation of strong ground motion due to active Sohna fault in Delhi, national capital region (NCR) of India: an implication for imminent plausible seismic hazard. Nat Hazards 104(3):2389–2408

Sharma ML (1998) Attenuation relationship for estimation of peak ground horizontal acceleration using data from strong-motion arrays in India. Bull Seismol Soc Am 88(4):1063–1069

Sharma ML, Douglas J, Bungum H, Kotadia J (2009) Ground-motion prediction equations based on data from the Himalayan and Zagros regions. J Earthq Engg 13:1191–1210

Sharma B, Chingtham P, Sutar AK, Chopra S, Shukla HP (2015) Frequency dependent attenuation of seismic waves for Delhi and surrounding area. India Ann Geophys 58(2):S0216

Shukla AK, Prakash R, Singh RK et al (2007) Seismotectonic implications of Delhi region through fault plane solutions of some recent earthquakes. Curr Sci 93:1848–1853

Shukla AK, Singh RK, Prakash R (2018) Instrumentation seismology in India. Advances in Indian earthquake engineering and seismology: contributions in honour of Jai Krishna. Springer, Cham, pp 19–33

Singh R (2020) Pandemic lockdown sensitizes New Delhi to earthquake risk. Temblor. https://doi.org/10.32858/temblor.087

Singh SK, Apsel RJ, Fried J, Brune JN (1982) Spectral attenuation of SH waves along the Imperial fault. Bull Seismol Soc Am 72:2003–2016

Singh RP, Aman A, Prasad YJJ (1996) Attenuation relations for strong seismic ground motion in Himalayan Region. Pure Appl Geophys 147(1):161–180

Singh SK, Ordaz M, Dattatrayam RS, Gupta HK (1999) A spectral analysis of the May 21, 1997, Jabalpur, India earthquake (Mw=5.8) and estimation of ground motion from future earthquakes in the Indian shield region. Bull Seismol Soc Am 89:1620–1630

Singh SK, Mohanty WK, Bansal BK, Roonwal GS (2002) Ground motion in Delhi from future large/great earthquakes in the central seismic gap of the Himalayan Arc. Bull Seismol Soc Am 92:555–569. https://doi.org/10.1785/0120010139

Singh SK, Garcia D, Pacheco JF, Valenzuela R, Bansal BK, Dattatrayam RS (2004) Q of the Indian shield. Bull Seismol Soc Am 94(4):1564–1570

Singh SK, Kumar A, Suresh G et al (2010) Delhi earthquake of 25 November 2007 (4.1): implications for seismic hazard. Curr Sci 99:939–947

Singh SK, Suresh G, Dattatrayam RS et al (2013) The Delhi 1960 earthquake: epicentre, depth and magnitude. Curr Sci 105:1155–1165

Srinagesh SSK, Arroyo D, Srinivas D, Suresh G, Suresh G (2021) Ground motion prediction equation for earthquakes along the Western Himalayan arc. Curr Sci. https://doi.org/10.18520/cs/v120/i6/1074-1082

Tiwari DK, Jha B, Kundu B, Gahalaut VK, Vissa NK (2021) Groundwater extraction-induced seismicity around Delhi region. India Scientific Reports 11(1):1–14

Verma RK, Roonwal GS, Kamble VP et al (1995) Seismicity of Delhi and its surrounding region. J Himalayan Geol 6:75–82. https://doi.org/10.1007/s13398-014-0173-7.2

Publisher's Note Springer Nature remains neutral with regard to jurisdictional claims in published maps and institutional affiliations.